CONCERNING THE SPACE CHARGE ACCUMULATION IN DC POWER CABLE JOINTS INSULATION

Cristina Stancu, Petru V. Notingher, Lucian Viorel Taranu

University Politehnica of Bucharest, 313 Splaiul Independentei Str., Bucharest, Romania

Abstract

After an analysis of the structure and properties of the DC joints insulation components, the generation mechanisms and the measurements methods of the space charge in DC multilayer joints are presented. Then, the equations used to calculate the charge accumulated at the homogeneous interfaces of the joints and the electric field are given.

To calculate the space charge density and the electric field, experiments on flat samples (XLPE and reductionEPDM) are performed and their dielectric properties are measured.

Finally, it is shown that the charge accumulation leads to local enhancements of the electric field and to degradation and lifetime reduction of joints.

Key words: *HVDC cable joints, aging, interfaces, space charge, electric field*

1. INTRODUCTION

Worldwide, in recent years there has been a considerable increase in electricity consumption (Jeroen 2013). As electricity is produced generally far from consumers, an important issue concerns its transportation with lowest cost and highest safety. There are two ways for electricity transportation: alternating current (AC) and direct current (DC). On land, electricity can be transmitted by overhead lines or underground cables, while for populated areas and for sub-sea transmission only cables are available.

AC cables have a number of disadvantages (conductor and insulation losses are relatively high, important electromagnetic pollution etc.), as opposed to the DC which has several major advantages: higher capacity of power transmission, lower conductor losses, no electromagnetic interference, no skin effect, reduced corona losses, relatively low magnetic field (below the maximum allowed of 400 mT) (Europacable 2011, Sharif 2012), reduced environmental impact, etc. Hovewer there are some disadvantages of DC cables: high cost of the DC/AC conversion stations (thyristors, IGBTs), the need to use harmonic filters etc. Anyway, for one DC cable kilometer is spend less than for an AC one (Larruskain 2005). In the recent years, the DC cables began to occupy a more important weight (Kim 2009). Among these are distinguished the DC lines which connect Xianjiaba to Shanghai (2071 km, ± 800 kV), Great Britain to France (64 km, ± 270 kV) and Norway (estimated for 2020, 711 km) etc. The line between France and Spain (4 cables of 64 km each, ± 320 kV) is under construction, and until 2020 the DC lines that connects Sweden and Norway, Denmark and Norway, Italy and Libya, Poland and Egypt, Great Britain-Germany and Egypt etc. will be operational (Europacable 2011). There is also a project for the construction of a submarine DC line that will connect Romania and Turkey (400 km ± 400 kV). It should be noted that in 2011 there were already in operation more than 1.000 kilometers of high voltage power cables in Europe (HVDC) (Europacable 2011).

The continuous development of DC network is lately required by the development of the clean energy sources, to connect the solar, wind, geothermal, marine etc. stations (Hjertberg 2013). This will become particularly important in the future because until 2100 the use of hydrocarbons (coal, oil and natural gas) will no longer be used to produce electricity (Kreutzer 2015). For areas where it exists already an AC network, the conversion of AC into DC lines is tried (Aghazadeh 2014).

High Voltage Direct Current (HVDC) transmission lines are mainly used when there is a need to transport high electrical power over long distances overland and/or in a controlled manner (in

submarine applications, connecting offshore wind farms etc.). Two HVDC land transmission technologies are used to carry electricity over long distances (Jeroense 2013):

a) HVDC overhead lines to carry high power (>1,000 MW) over distances above 200 km;

b) HVDC underground cables to carry medium and high power (100 MW – 1,000 MW) over distances above 50 km.

These two transmission technologies are compatible and can be combined. The transition from the overhead line to the underground cable is realized via a transition connection installed in a transition yard. HVDC undergrounding can safely transport high power loads over long distances with minimal losses. In addition to this transport efficiency, only a limited number of cables are required, hence allowing narrow trenches.

In addition to oil-filled cables, two cable technologies are commercially available for HVDC: mass impregnated (MI) cables with a combination of kraft paper and oil based compound as insulation system (Fig. 1) and extruded cables with cross linked polyethylene (XLPE) as insulation material (Fig. 2) (Hjertberg 2013, Hondaa 2013, Jeroense 2013).



Fig. 1. DC power cable with MI.



Fig. 2. DC power cable with XLPE.

For land use, the HVDC cable length is limited by logistical constraints regarding transportation, access and installation. Consequently, the maximum length is dependent on the cable diameter and weight. HVDC cables can be directly buried into the ground or installed in tunnels, ducts or pipes to respond to requirements from surroundings, and/or to enhance protection against external damage (Europacable 2011).

Since sections of DC high voltage cables have reduced lengths (1 ... 10 km), transporting energy over long distances requires several sections (connected by joints). There are two types of joints cables: with paper insulation and oil-polymer insulation. Joints with paper-oil insulation (MI) are used, especially for distances below 100 km, 500 kV and power voltages below 800 MW. For longer distances and higher voltages and power, great efforts have been made in recent years to achieve joints with extruded polymer insulation: XLPE, EPDM, silicone rubber, etc. Their use offers many advantages, such as higher operating temperature of the conductor, easier combination of the joints, minimal maintenance costs etc.

Joints for high voltage cables with polymeric insulation have relatively complex structures. Besides the conductor, the joints have a polymeric insulation - successive layers of polymeric materials (cross-linked polyethylene - XLPE, ethylene-propylene rubber - EPR rubber, ethylene propylene diene monomer - EPDM, silicone rubber), semiconductor layers (XLPE + carbon black) and deflector cones to control the field lines etc. (Fig. 3) (Bartnikas 2000**)**.

The joints with polymer insulation can be performed in situ directly on cables in operation or, more simply, in specialized manufactories (and then mounted on cables). Figures 3 and 4 show the pre-formed (Fig. 3) (Bartnikas 2000) or prefabricated joints (Fig. 4) (Parpal 1996). A joint in situ can be made by extrusion, in which case the same resin is used (polymer) for cable insulation (Fig. 5) (Bartnikas 2000). In this situation impurities and cracks (cavities) can occur in joint insulation reducing its performance. Joints are generally incorporated in joint bays (metal skeleton) which protect them after the installation against mechanical accidental stresses and humidity (Fig. 6) (Europacable 2011). Joint bays can be directly buried into the ground, surrounded only by a sand blending. If required, joint bays may be placed into an underground structure.

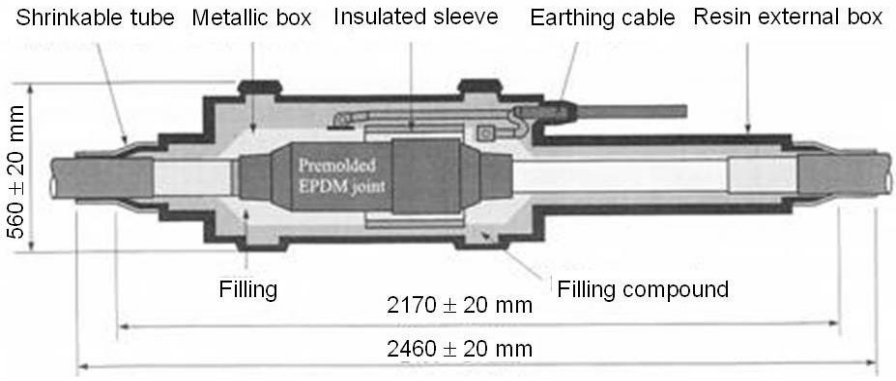


Fig. 3. Section through a preformed joint for power cables with voltage of 500 kV (Bartnikas 2000).

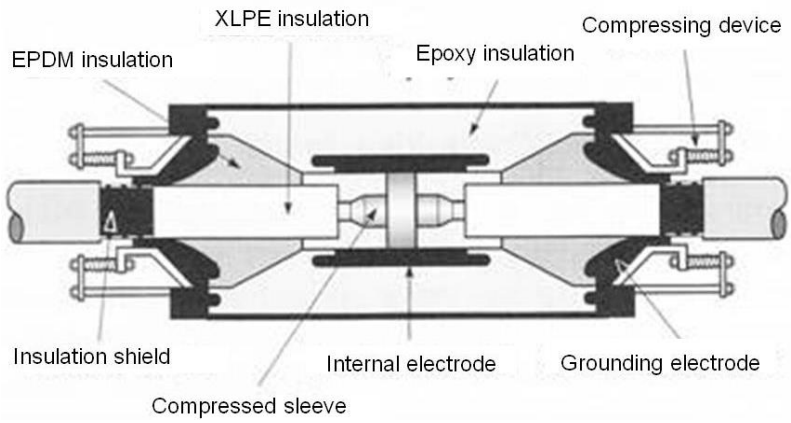


Fig. 4. Prefabricated joint structure (Parpal 1996).

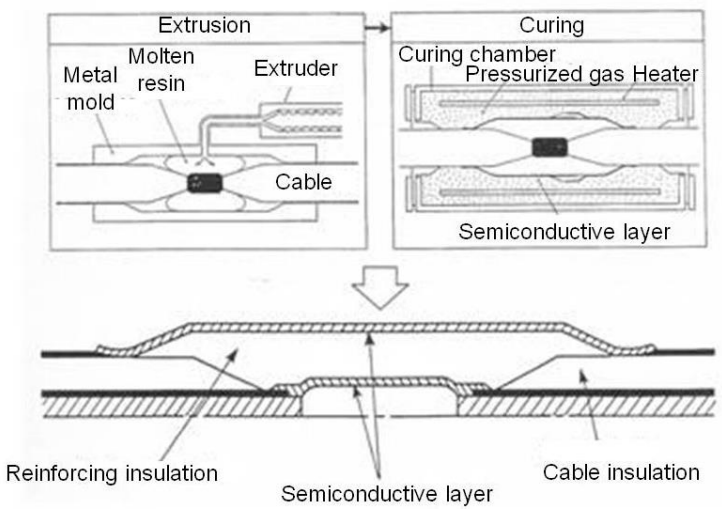


Fig. 5. Joint formed by extrusion in situ (Bartnikas 2000).

To connect the cable to different devices (converters, switchgears, gas insulated switchgears, etc.) different terminations (with similar structures as the joints) are used (Pfisterer 2015).

Joints are considered the most vulnerable components of a DC line. The statistics made in recent years shows that joints are responsible for 55 % of premature removal from operation of transmission and distribution lines of electricity (Europacable 2011). Therefore, joints are subjected to the same tests and must meet the same requirements as the cables themselves (Parpal 1996). Research done on DC power lines refers lately more on these products (CIGRE 2016). Research topics concerns, on one hand, the study of electrical properties of the DC joints insulation components (i.e., estimation of the lifetime) and, on the other hand, the space charge accumulation within them.

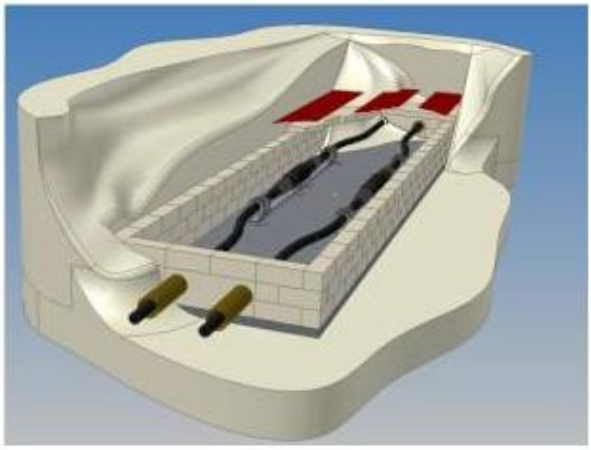


Fig. 6. Joint Bay (Europacable 2011).

2. GENERATION AND SPACE CHARGE MEASUREMENT

Regardless of the manufacturing and the type of polymer used for insulation (identical or different from those used for cable insulation), all insulation joints contain space charge. It is produced during the cross-linking process (methane, acetophenone and cumyl alcohol etc.), by injection of charge carriers at the interface semiconductor/insulator, due to polymer degradation, partial discharges, etc. (Bodega 2006, Hjertberg 2013, Montanari, 2005, Suh 1994). On the other hand, if the polymeric

materials which are part of the joint have different physical and electrical properties, during the cables operation superficial charge of density ρ_s occurs at the insulation-insulation interfaces (Bodega 2006 a, Bodega 2006 b, Notingher 2005, Taranu 2015), leading to the apparition of an additional polarization (inhomogeneous polarization) (Notingher 2005). Also, the space charge accumulates at the interfaces with the semi-conductors layers, the interfaces between amorphous and crystalline areas in the insulation and around defects or impurities (areas particularly prone to trap of charges) (Hondaa 2013). The temperature variation in joint insulations (higher near the conductor and lower outside) makes the space charge accumulation easier, increasing the superficial charge density ρ_s (Fu 2007). These variations are pronounced, especially in regions where the temperature differences day/night and summer/winter, are relatively important. In these cases, the joint insulations are subjected to thermal ageing by heating/cooling cycles, and, thus, ρ_s increases (Amyot 2001).

The values of charge density ρ_s depend on the chemical nature and physical structure of the insulations, electrical properties of the polymeric materials used, and, especially, on their time variation under the action of the electrical and thermal operating stresses.

A simple relation to calculate the charge density $\rho_s(t)$ separated at the interface between two insulating plates (1 and 2) of thickness g_1 and g_2 situated between the armatures of a plane capacitor, at the instant t after the DC voltage application is:

$$\rho_s(t) = \frac{\varepsilon_1\sigma_2 - \varepsilon_2\sigma_1}{\sigma_1 g_2 + \sigma_2 g_1} U\left[1 - \exp\left(-\frac{t}{\tau}\right)\right], \qquad (1)$$

where $\tau = \frac{g_1\varepsilon_2 + g_2\varepsilon_1}{g_1\sigma_2 + g_2\sigma_1}$, $\sigma_{1,2}$ and $\varepsilon_{1,2}$ represents the conductivities and permittivity's of the insulations 1 and 2 (Morshuis 2013, Stancu 2014) .

The increase of the charge density ρ_s leads to enhanced local values of E contributing to partial discharges intensification and insulation degradation (and therefore to increased values of the charge carriers concentration and space charge) (Seghier 2010). It also increases the probability of electrical and water trees inception, respectively the premature breakdown of the insulations. As consequence, the electricity to some consumers is interrupted and some material damages and a reduction of the electricity quality occur.

On the other hand, in DC the space charge accumulated in joint insulations is not canceled instantaneously by the voltage switch off and remains stored for large time intervals (even weeks). The size of these intervals depends on the charge carriers mobility, traps depth where the charge is fixed (and, thus, the value of the activation energy), temperature etc. This residual charge produces a high enough residual electric field (up to values several times higher than those existing in the absence of charge (Stancu 2013, Taranu 2015), which can produce a premature electrical ageing of the insulation (by partial discharges and/or electrical trees) (Stancu 2009). For these reasons, knowledge of the space charge density values and electric field repartition at any time during the joint operation is a method to estimate the behavior in time of the joints and their lifetime (respectively the necessary time to switch off the voltage to replace the joints).

There are many researches regarding the influence of the thermal stresses on the degradation of the insulations and space charge accumulation (Namouchi 2007, Tsekmes 2012, Ve 2013). The electrical stresses (especially by the action of partial discharges) contribute, too, to their degradation. As consequence, in the polymeric insulations new charge carriers occur, both inside the homogeneous areas and at their interfaces (Taranu 2015).

More precise measurements of the space charge developed in polymer cable insulations have been a research topic of numerous groups from universities and research centers. Methods and equipments were realized allowing the space charge determination, on flat and cylindrical samples but also on cables in operation (Abou-Dakka 1997, Abou-Dakka 2004, Boggs 2004, Montanari 2005). Among the

methods used to detect and measure the space charge the electro-optics method (based on Kerr effect), electro-acoustic method (Pulsed Electroacustic Method – PEM), pressure pulse method (Pressure Pulse Method – PPH) or (Laser Induced Pressure Pulse – LIPP, respective, Laser Intensity Modulation Method – LIMM) and thermal method (Thermal Wave Method – TWM) etc. (Notingher 2005) may be remarked.

The Thermal Step Method (developed by University of Montpellier II – France) is concerned with the diffusion of a heat step applied to one side of the sample. The method allows the space charge measurements on plane and cylindrical samples and on operating cables (using high intensity electric currents to generate heat wave) (Agnel 2013, Castellon 2005, Notingher 2001, Notingher 2009, Toureille 1991).

The principle of this method is relatively simple (Toureille 1991). Thus, is considered an isolated plate of thickness g, provided with two electrodes whose abscissa are $x = 0$, and $x = g$ (Fig. 7) (Stancu 2008) and it is assumed that: a) the plate is homogeneous, b) the thickness g is much smaller than the length (L) and width (l) (i.e., $g << \sqrt{S}$, $S = L.l$ – being the flat plate surface area) and c) electric field is constant in a plane parallel to the electrode surfaces. The sample is short-circuited (by the conductor Γ, Fig. 7) and is at the temperature T_0.

A charge Q_i situated in abscissa point x_i is considered. As the system sample/electrodes/wire is in electrostatic equilibrum, the charge Q_i induces at the electrodes the charge images Q_1 and Q_2 (Stancu 2008):

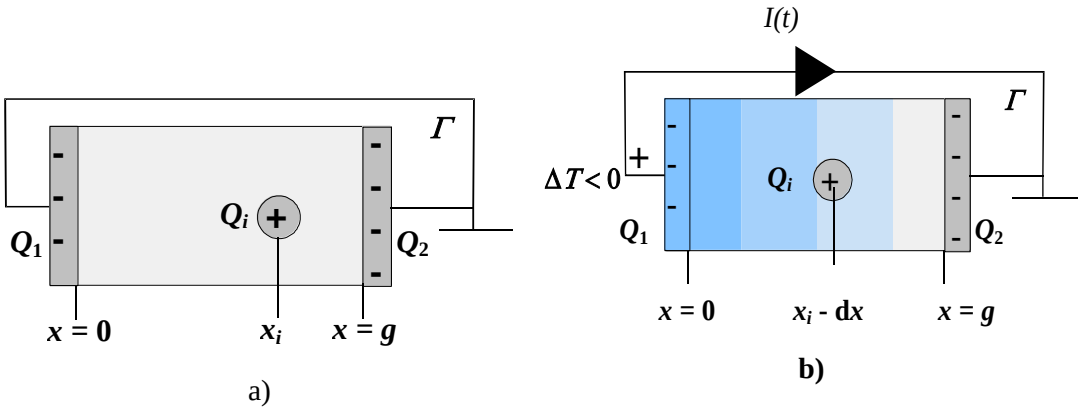


Fig. 7. Principle of the thermal step method: a) Sample in equilibrum at T_0;
b) Applying of a thermal step ΔT.

$$Q_1 = -\frac{g - x_i}{g} Q_i \qquad (2)$$

$$Q_2 = -\frac{x_i}{g} Q_i \,. \qquad (3)$$

If a thermal step $\Delta T = T - T_0$ is applied on one sample face, the thermal front propagation generates local variations of the temperature in time ($T(x,t)$), electrical permittivity ($\varepsilon(x,t)$) and position of the charge Q_i (by thermal expansions or contractions), resulting (Stancu 2008):

$$Q_2(t) = -Q_i \frac{x_i}{g}\left[1 + \frac{\alpha}{x_i}\int_0^{x_i}\Delta T(x,t)\mathrm{d}x - \frac{\alpha}{g}\int_0^{g}\Delta T(x,t)\mathrm{d}x\right], \quad (4)$$

where

$$\alpha = \frac{1}{x} - \frac{1}{\varepsilon}\frac{\mathrm{d}\varepsilon}{\mathrm{d}T}. \quad (5)$$

Variation of the image charge determines an electrical current occurence. This current is known as thermal wave current of intensity:

$$i(t) = -\frac{\mathrm{d}Q_2(t)}{\mathrm{d}t}. \quad (6)$$

Knowing the current $i(t)$ and spatial distribution of temperature ($T(x,t)$), the amount of charge Q_i and its position x_i can be determined.

By integration in the entire sample, the total current $I(t)$ and, then, the space charge density $\rho(x)$ are obtained:

$$I(t) = -\alpha C\int_0^{g} E(x)\frac{\partial\Delta T(x,t)}{\partial t}\mathrm{d}x \quad (7)$$

$$\rho(x) = \varepsilon\frac{\mathrm{d}E(x)}{\mathrm{d}x}, \quad (8)$$

where $E(x)$ is the electric field in the plane of abscissa x, C – capacity of the sample before applying the thermal step and α - a factor that accounts the variation of the permittivity with temperature (equation (4)) (Stancu 2008).

Therefore, by measuring the thermal step current $I(t)$ (by using a picoammeter (pA), Fig. 8), the electric field $E(x)$ and the space charge density $\rho(x)$ in each abscissa point x can be calculated (using the equation (8)) (Toureille 2013).

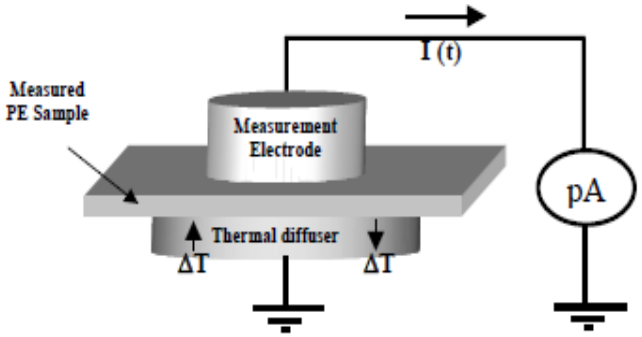


Fig. 8. Measurement of the space charge in a flat sample (Toureille 2013).

This paper presents the results regarding the experimental determination of the conductivities and permittivities of a DC joint composite insulation made from three polymeric layers. Also, the superficial charge density and electric field in absence and presence of the space charge are calculated and presented.

3. COMPUTATION OF THE ELECTRIC FIELD

To calculate the electric field, a flat capacitor having as dielectric the sample C, made from two square plates from XLPE with side l = 100 mm amd thickness g_1 = 1.1 mm and a square plate from EPDM having the same length l = 100 mm and thickness g_2 = 0.8 mm (Fig. 9) was considered. Computations were done in a domain $D = D_1 \cup D_2 \cup D_3$ (Fig. 9), consisting of sub domain D_1 (corresponding to the first XLPE layer, of thickness g_1, relative permittivity ε_{r1} and conductivity σ_1) – delimited by the surfaces S_1 ($S_1 = l^2$) and S_{12}, D_2 (corresponding to EPDM layer, of thickness g_2, relative permittivity ε_{r2} and conductivity σ_2) –delimited by the surfaces S_{12} and S_{23} and D_3 (corresponding to the second XLPE layer, of thickness g_3, relative permittivity $\varepsilon_{r3} = \varepsilon_{r1}$ and conductivity $\sigma_3 = \sigma_1$) – delimited by the surfaces S_{23} and S_2 ($S_2 = l^2$). A value of surface potential V_1 = 15 kV has been assigned to S_1 , whilst a value V_2 = 0 (ground potential) has been set on S_2.

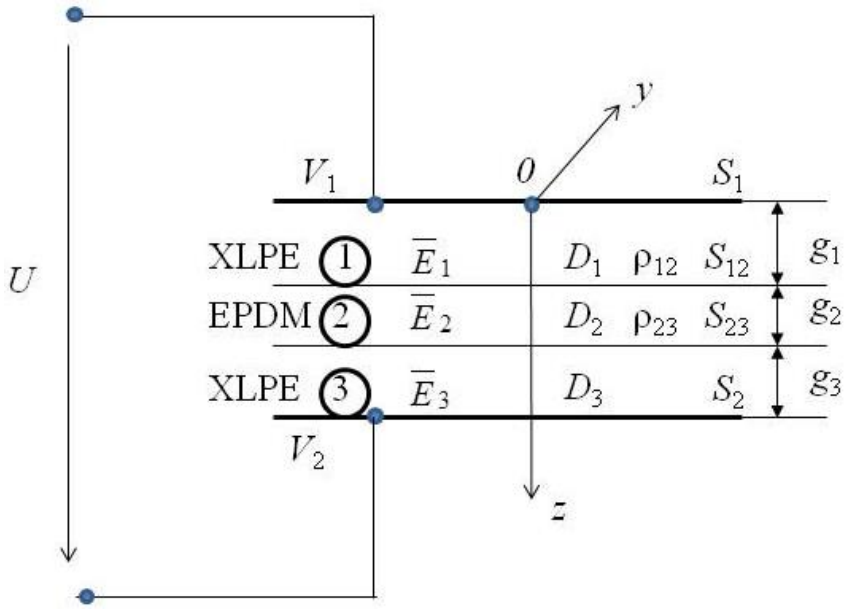


Fig. 9. Computation domain.

3.1. Equations

Considering the domain D as linear, isotropic and inhomogeneous, respectively

$$\overline{D}(P) = \varepsilon(P)\overline{E}(P), \quad P \in D \tag{9}$$

$$\overline{J}(P) = \sigma(P)\overline{E}(P), \quad P \in D, \tag{10}$$

and the quasi-stationary field regime, the following equations were used:

- Electric flux law: $\operatorname{div}\overline{D}(P) = \rho_v(P), \quad P \in D$, (11)

- Charge conservation law: $$\operatorname{div}\overline{J}(P)+\frac{\partial \rho_v(P)}{\partial t}=0,\ P\in D \quad , \qquad (12)$$

- Potential theorem: $$\overline{E}(P)=-\operatorname{grad}V(P),\ P\in D, \qquad (13)$$

where $\overline{D}(P)$ represents the electric induction, $\overline{J}(P)$ - electric current density, $\overline{E}(P)$ - electric field, and $V(P)$ – electric potential, ε(*P*) – electrical permittivity and σ(*P*) – electrical conductivity in a point $P\in D$ at time *t*.

3.2. Boundary conditions

On the surfaces S_1 and S_2 Dirichlet conditions were imposed at each time *t*:

$$V(M)=V_1,\quad M\in S_1, \qquad (14)$$

$$V(M)=V_2,\quad M\in S_2. \qquad (15)$$

On the discontinuity surfaces S_{12} and S_{23} the following conditions were imposed at each time *t*:

$$\overline{n}_{12}\left(\overline{J}_2(M)-\overline{J_1}(M)\right)+\frac{\partial \rho_s(M)}{\partial t}=0,\quad M\in S_{12}, \qquad (16)$$

$$\overline{n}_{23}\left(\overline{J}_3(M)-\overline{J_2}(M)\right)+\frac{\partial \rho_s(M)}{\partial t}=0,\quad M\in S_{23}, \qquad (17)$$

$$\left(\varepsilon_1\frac{\partial V_1(M)}{\partial n_{12}}-\varepsilon_2\frac{\partial V_2(M)}{\partial n_{12}}\right)=\rho_{s1}(M),\ M\in S_{12}, \qquad (18)$$

$$\left(\varepsilon_2\frac{\partial V_2(M)}{\partial n_{23}}-\varepsilon_3\frac{\partial V_3(M)}{\partial n_{23}}\right)=\rho_{s2}(M),\ M\in S_{23}, \qquad (19)$$

where $\varepsilon_{1,2,3}=\varepsilon_{r1,2,3}.\ \varepsilon_0$ and ε_0 is the vacuum permittivity.

3.3. Initial conditions

The following initial condition was written for the superficial charge density ρ_s:

$$\rho_s(M)\big|_{t=0}=0,\ M\in S_{12}\cup S_{23}. \qquad (20)$$

3.4. Material properties

The values of DC conductivity measured at *U* = 1000 V (σ) and the real part of complex relative permittivity (designated as relative permittivity - ε_r) measured at 50 Hz, for samples A and B, unaged and thermally aged at 105 ºC are presented in Table 1.

Table 1. DC Conductivity (at t = 2700 s and U = 1000 V) (σ) and relative permittivity (at 50 Hz) (ε_r) values, for samples A and B

Sample	σ (S/m)	ε_r
A (XLPE), unaged	$1.48 \cdot 10^{-15}$	2.41
A (XLPE), aged 240 h	$2.51 \cdot 10^{-15}$	2.45
A (XLPE), aged 480 h	$1.17 \cdot 10^{-15}$	1.81
B (EPDM), unaged	$1.26 \cdot 10^{-14}$	3.32
B (EPDM), aged 240 h	$4.55 \cdot 10^{-15}$	3.25
B (EPDM), aged 480 h	$1.10 \cdot 10^{-14}$	2.59

4. EXPERIMENTS

To measure the permittivity and electrical conductivity (in AC and DC), flat samples from XLPE (A), EPDM (B) and multilayer XLPE/EPDM/XLPE (C) with different dimensions (Table 2) were used. The samples were manufactured by Cablel Romania and were obtained from pellets pressed at T = 180 ºC and pressure p = 200 bar for 10 minutes.

Table 2. Dimensions of samples

Sample	DC measurements	AC measurements
A	100x100x1.1 (mm)	40x40x1.1 (mm)
B	100x100x0.8 (mm)	40x40x0.8 (mm)
C	100x100x3 (mm)	40x40x3 (mm)

All samples were thermally conditioned at T = 60 ºC for 48 h and, then, the values of permittivity and electrical conductivity were measured. Further, groups of three samples A, B and C were placed in an oven for fast thermal ageing. Choosing the aging temperature was made so that it is below the softening temperature of the sample, determined experimentally by DSC (118 °C to 139 °C for XLPE and EPDM) (Stancu 2014). After 240 and 480 hours respectively, the samples were removed from the oven and the values of permittivity and electrical conductivity were measured.

To determine the DC electrical conductivity σ(t), the absorption $i_a(t)$ and resorption $i_r(t)$ currents were measured (up to 4 h) on samples A, B and C with a Keithley 6517 electrometer under a voltage U_0 = 100…2000 V and the temperatures between 25 and 70 ºC (Notingher 2010, Stancu 2013).

The components of the complex relative permittivity were measured on square plates (of side b = 40 mm) with a Novocontrol Impedance Analyzer (Stancu 2011). The applied voltage was 1 V and the frequency between 1 mHz and 1 MHz.

5. RESULTS

5.1. Electrical conductivity

In Figures 10…12 the time variations of the absorption $i_a(t)$ and resorption $i_r(t)$ currents on unaged and thermally aged samples A, B and C, measured at U = 1000 V and T = 28 °C are presented. The absorption and resorption currents have 4, respectively 3 components:

$$i_a(t) = i_i(t) + i_p(t) + i_{sc}(t) + i_c(t) \quad (21)$$

$$i_r(t) = i_d(t) + i_{dp}(t) + i'_{sc}(t) \quad (22)$$

where $i_i(t)$ is the charging current of the capacitor with vacuum as dielectric, $i_p(t)$ - the polarization current, $i_{sc}(t)$ - the space charge current, $i_c(t)$ - the conduction current, $i_d(t)$ - the discharge current of the vacuum dielectric capacitor, $i_{dp}(t)$ – the depolarization current and $i_{sc}'(t)$ – the space charge current (Notingher 2010).

It is found that, for all cases, the currents $i_a(t)$ and $i_r(t)$ decrease in time due to the reduction of polarization $i_p(t)$, depolarization $i_{dp}(t)$ and space charge $i_{sc}(t)$, respectively $i_{sc}'(t)$ components (Notingher 2010).

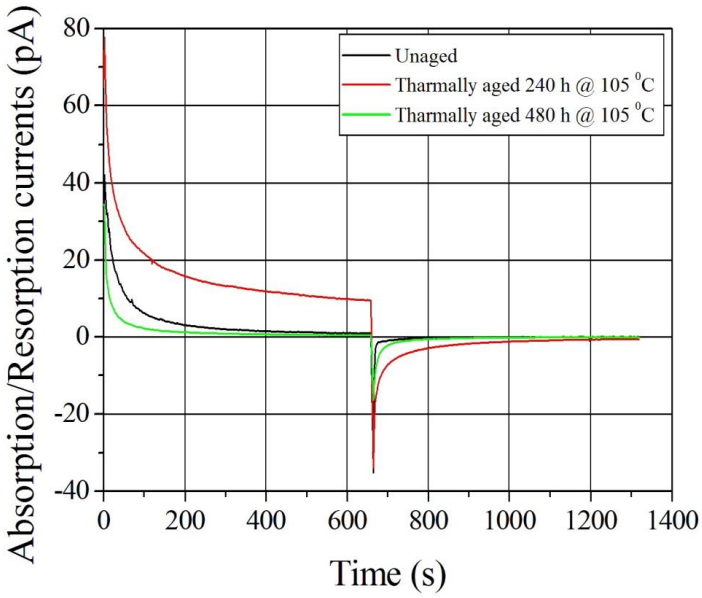


Fig. 10. Variation of absorption/resorption currents with time for A (XLPE) samples (U = 1000 V, T = 28 °C).

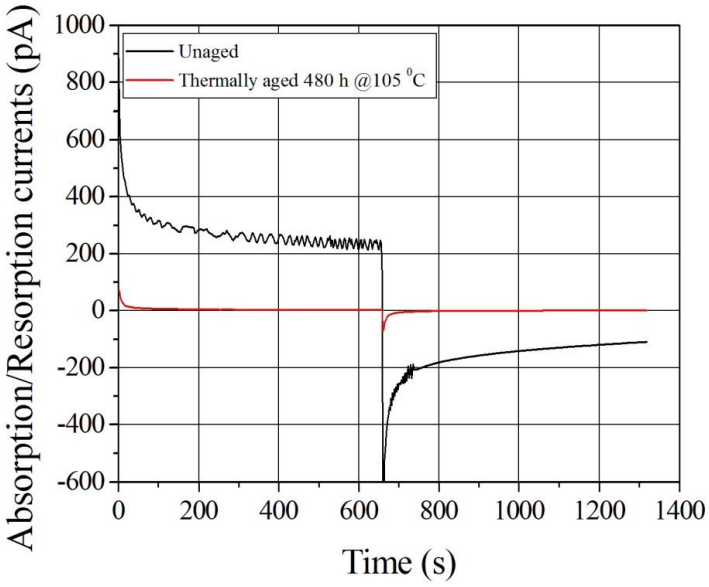


Fig. 11. Variation of absorption/resorption currents with time for B (EPDM) samples (U = 1000 V, T = 28 ^{0}C).

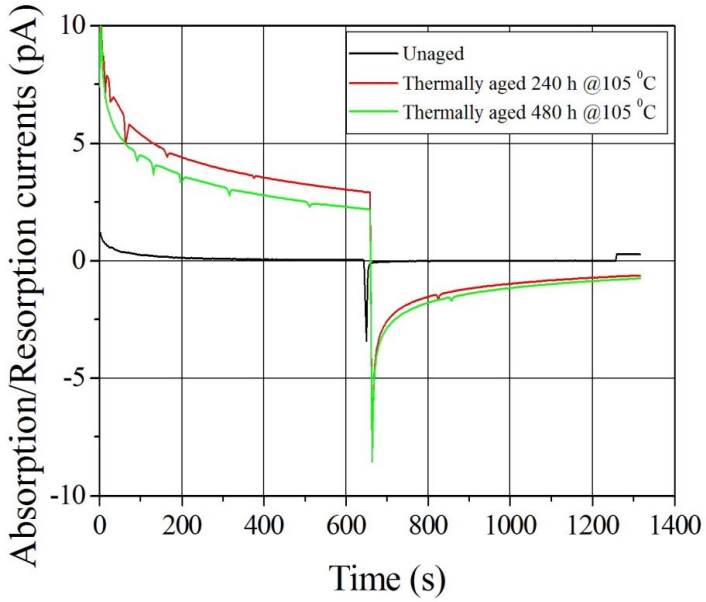


Fig. 12. Variation of absorption/resorption currents with time for C (XLPE/EPDM/XLPE) samples (U = 1000 V, T = 28 0C).

Knowing the absorption $i_a(t)$ and resorption $i_r(t)$ currents, the conductivity values $\sigma_m(t)$ were calculated with the equation:

$$\sigma_m(t) = \frac{i_a(t) - i_r(t)}{U} \cdot \frac{g}{S}, \tag{23}$$

where g is the thickness and S – the surface area of the tested sample (Stancu 2014).

Time variations of the electrical conductivity ($\sigma_m(t)$), for unaged and thermally aged samples are presented in Figures 13-15. It was found that, for all samples, the conductivity reduces in time. This is obviously due to the reduction in time of the polarization and space charge currents.

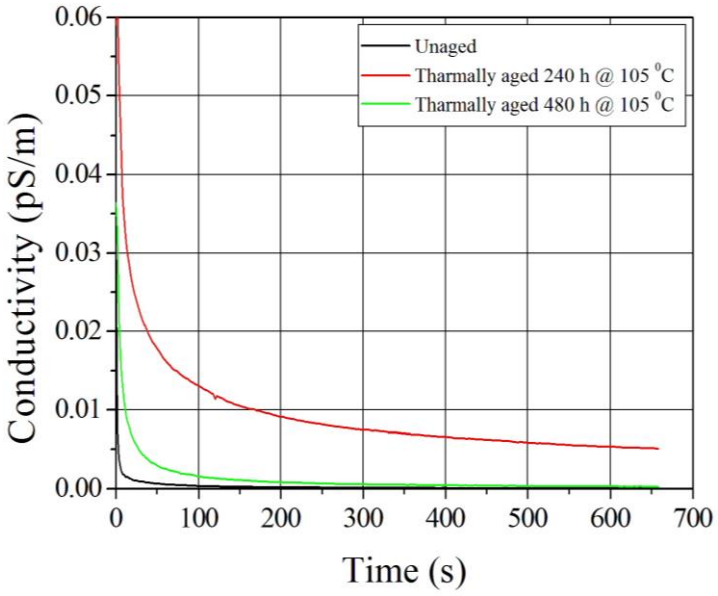


Fig. 13. Variation of the electrical conductivity $\sigma_m(t)$ with time for A (XLPE) samples (U = 1000 V, T = 28 ^{0}C).

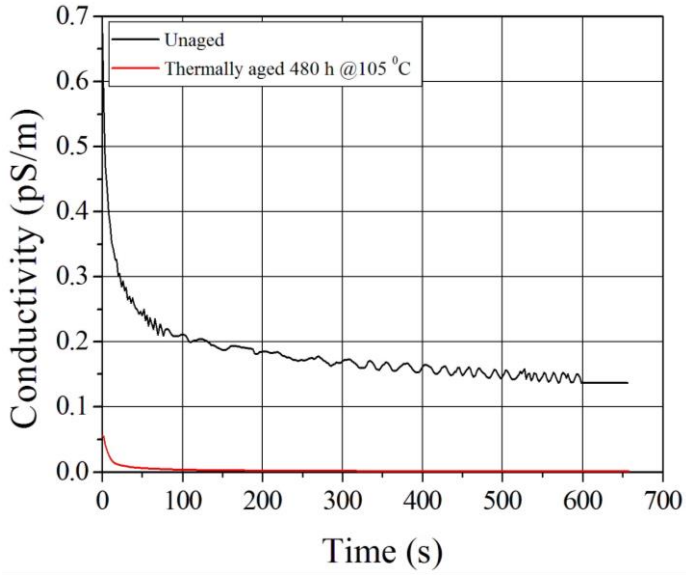


Fig. 14. Variation of the electrical conductivity $\sigma_m(t)$ with time for B (EPDM) samples (U = 1000 V, T = 28 ^{0}C).

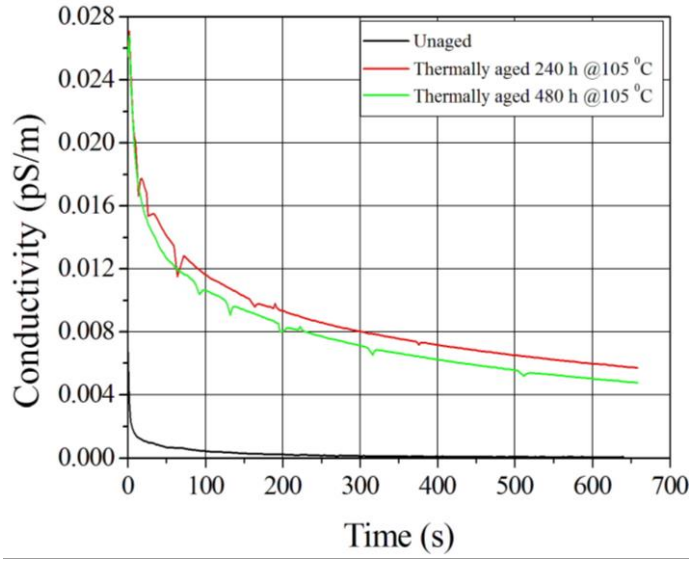


Fig. 15. Variation of the electrical conductivity $\sigma_m(t)$ with time for C (XLPE/EPDM/XLPE) samples (U = 1000 V, T = 28 ^{0}C).

By using the measured values of the conductivities on samples XLPE (σ_A) and EPDM (σ_B) at a time t, the conductivity of the multilayer sample XLPE/EPDM/XLPE at the time t (σ_C) is calculated with the equation:

$$\sigma_C = \frac{\sigma_A \sigma_B (2g_1 + g_2)}{2g_1\sigma_2 + g_2\sigma_1}, \qquad (24)$$

where $g_{1,2}$ represents the thickness of the samples A and, respectively, B.

In Tables 3 and 4 the measured conductivity (σ_m) values for 60 and 300 s after the voltage application, for unaged (τ = 0) and thermally aged (τ = 480 h) samples A, B and C and calculated one (σ_c) for samples C are presented. For multilayer samples C, comparing the calculated values with the measured ones (Table 3), it was found that the measured values are, generally, greater than the calculated ones. It results, that for this sample an absorption current greater than those corresponding to the conductance of the three layers connected in parallel was measured. This supplementary current could be due to a supplementary charge absorbed by the capacitor and fixed on the two interfaces of the multilayer sample (XLPE/EPDM), having the superficial charges ρ_{s1} and ρ_{s2}.

Separation of the space charge at the sample interfaces will be confirmed by the space charge measurement on samples C by using the Thermal Step Method.

Table 3. Values of the electrical conductivity σ_m for A and B samples, measured at the moment *t* after the voltage application *U*

Sample	*t* (s)	σ_m (S/m)	
		$\tau = 0$	$\tau = 480$ h
A (XLPE)	60	$6.48 \cdot 10^{-16}$	$1.21.10^{-14}$
	300	$1.18 \cdot 10^{-16}$	$7.12 \cdot 10^{-15}$
B (EPDM)	60	$2.83 \cdot 10^{-13}$	$8.87 \cdot 10^{-15}$
	300	$1.70 \cdot 10^{-13}$	$1.64 \cdot 10^{-15}$
C (XLPE/EPDM/XLPE)	60	$1.50 \cdot 10^{-15}$	$1.2 \cdot 10^{-14}$
	300	$1.00 \cdot 10^{-16}$	$7.00 \cdot 10^{-15}$

Table 4. Values of the electrical conductivity calculated σ_c and measured σ_m for C samples at the moment *t* after the voltage application *U*

τ (h)	*t* (s)	σ_c (S/m)	σ_m (S/m)
0	60	$8.157.10^{-16}$	$1.5.10^{-15}$
0	300	$1.603.10^{-16}$	1.10^{-14}
480	60	$1.102.10^{-14}$	$1.2 \cdot 10^{-14}$
480	300	$3.765.10^{-15}$	$7.00 \cdot 10^{-15}$

5.2. Electrical permittivity

In Figures 16-17 the variations of the real part of complex permittivity (knows as relative permittivity) with the frequency, for the samples A and B are presented. It was found that, for both samples, the relative permittivity decreases with the frequency increase, more for EPDM samples and less for XLPE ones. This is due to the increase of the polar species concentration (radicals and molecular end chains) that are oriented by the electric fields of lower frequencies, contributing to the increase of the electric polarization (and, hence, the permittivity) of the samples (Notingher 2005).

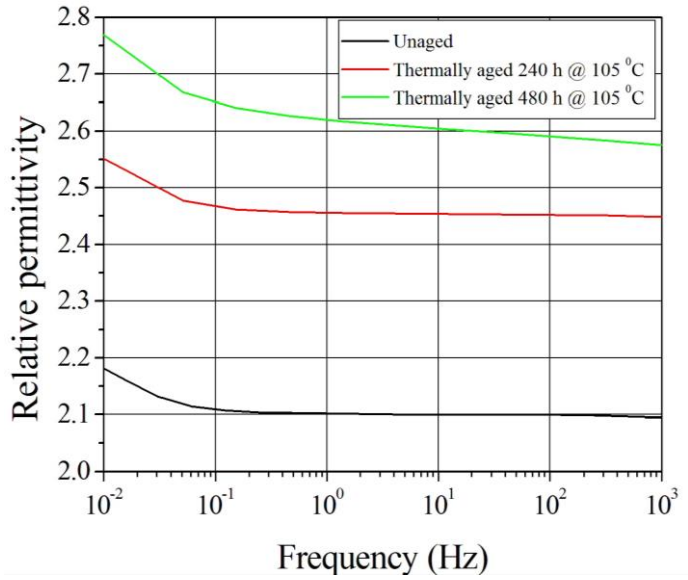


Fig. 16. Variation of the relative permittivity with frequency for XLPE (A) samples (U = 1 V, T = 28 ^{0}C).

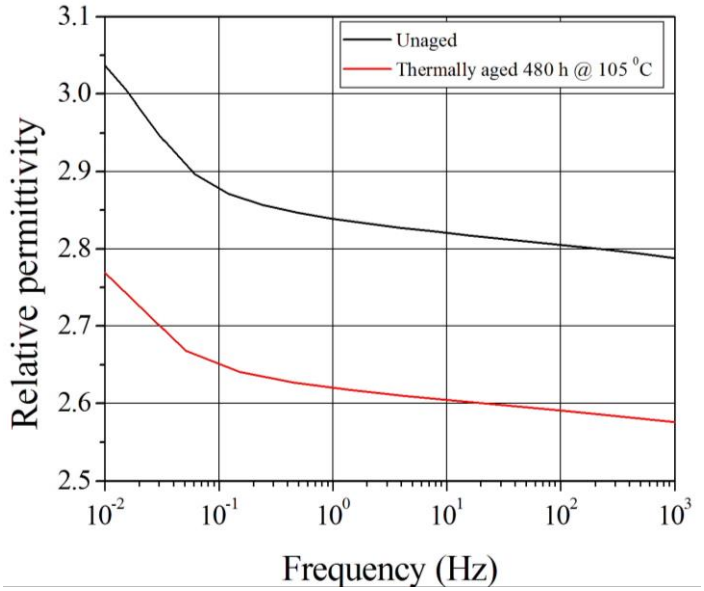


Fig. 17. Variation of the relative permittivity with frequency for EPDM (B) samples (U = 1 V, T = 28 ^{0}C).

5.3. Computation of the electric field

Computation of the electric field was done in the domain $D = D_1 \cup D_2 \cup D_3$ related to the multilayer sample C (Fig. 9), using the equations (9)…(20) and COMSOL MULTIPHYSICS software. The calculation procedure has three steps:

a) Computation of the initial values of the electric field in the absence of the volume charge density ($\rho_v(z) = 0$) and before the superficial charge separation on the interfaces S_{12} and S_{23}.

For that, the following equations were used (UEFISCDI 2016):

$$E_1(t) = b' + a'' e^{-t/\tau_2} + c e^{-t/\tau_1}$$
$$E_2(t) = a e^{-t/\tau_2} + b$$
$$E_3(t) = b'' - a''' e^{-t/\tau_2} - c' e^{-t/\tau_1} \quad (25)$$

where $a''' = \frac{g_1 a'' + g_2 a}{g_3}$, $a'' = \frac{a'\tau_2}{\tau_2 - \tau_1}$, $b'' = \frac{U - g_1 b' - g_2 b}{g_3}$, $a' = \frac{a}{\sigma_1}(\sigma_2 - \frac{\varepsilon_2}{\tau_2})$, $b' = b\frac{\sigma_2}{\sigma_1}$, $c' = c\frac{g_1}{g_3}$,

$a = U(\frac{\varepsilon_1}{\varepsilon_1 g_2 + 2\varepsilon_2 g_1} - \frac{\sigma_1}{\sigma_1 g_2 + 2\sigma_2 g_1})$, $b = U\frac{\sigma_1}{\sigma_1 g_2 + 2\sigma_2 g_1}$, $c = U\frac{\varepsilon_2}{\varepsilon_1 g_2 + 2\varepsilon_2 g_1} - a'\frac{\tau_2}{\tau_2 - \tau_1} - b'$,

$\tau_1 = \frac{\varepsilon_1}{\sigma_1}$ and $\tau_2 = \frac{\varepsilon_1 g_2 + 2\varepsilon_2 g_1}{\sigma_1 g_2 + 2\sigma_2 g_1}$.

b) Computation of the volume $\rho_v(z)$ and surface ρ_s charge densities. It was considered that in the domains D_1 and D_3 there is a volume space charge that varies with the z – coordinate according to the equations:

$$\rho_v(z) = \rho_{v01} e^{-c_1 z}, \quad \text{for } z \in (0, g_1)$$
$$\rho_v(z) = \rho_{v02} e^{-c_2(z_{max} - z)}, \quad \text{for } z \in (g_1 + g_2, z_{max}) \quad (26)$$

where $z_{max} = g_1 + g_2 + g_3$, c_1, c_2 and $\rho_{v01,2}$ are known.

Superficial charge density values at the interfaces S_{12} (ρ_{s1}) and S_{23} (ρ_{s2}) were computed using the equations:

$$\rho_{s1} = \varepsilon_1 E_1(g_1) - \varepsilon_2 E_2(g_1) \quad (27)$$
$$\rho_{s2} = \varepsilon_2 E_2(g_1 + g_2) - \varepsilon_1 E_3(g_1 + g_2)$$

obtained from the equations (18) - (19).

c) Computation of the numerical values of the electric field. To calculate the electric field E in the absence of the charge, the equations (25) were used.

d) With the obtained values for E, the ρ_{s1} and ρ_{s2} were computed. With COMSOL MULTIPHYSICS software and using ρ_{s1}, ρ_{s2} and ρ_v values (given by (26)) the values of E (respectively $E^1_{1,2,3}$) have been computed again in the three sub-domains $D_{1,2,3}$. Then, the values of ρ_{s1}, ρ_{s2}, and $E^2_{1,2,3}$ were computed again and the iterative process continues until the difference between two consecutive values of $E_{1,2,3}$ in the same point are smaller than 0.1 %.

In Figure 18 the variation of the electric field E with the z – coordinate in the domain D – that correspond to an unaged sample C – in the absence of the space charge, for U = 15 kV, ρ_{s1} = 0.12 mC/m^2, ρ_{s2} = - 0.12 mC/m^2, ρ_{v01} = 2 C/m^3, ρ_{v02} = - 2 C/m^3, $c_1 = c_2 = 11.5 \cdot 10^3$ m^{-1} is presented. It was found, as was expected, that in the absence of the charge the electric field is constant inside the sub-domains $D_{1,2,3}$ and has variations only at the interfaces between them (S_{12} and S_{23}) (blue curve, Fig. 18). These variations are due to the permittivity values that are different for the sub-domains $D_{1,2,3}$ (ε_r = 2.1 in $D_{1,3}$ and ε_r = 2.82 in D_2). The charge separation at the interfaces S_{12} and S_{23} leads to an important modification of E in the sub-domains D_1 and D_3 (Fig. 17, black curve), with about 28 %.

If the volume charge density is present in the sub-domains D_1 and D_3 (for example, injected by the electrodes) E increases significantly, especially in the electrodes vicinities (with about 91 %) (Fig. 17, red curve). Change the volume space charge sign leads to the reduction of E in the sub-domains D_1 and D_3 with about 31 % (Fig. 17, green curve). Therefore, the space charge accumulation (at the

sample interfaces) leads to the increase of the electric field above the critical values E_c for partial discharges and/or electrical trees initiation (E_c = 3 kV/mm) (Taranu 2015). Different mechanisms of multilayer insulation may be initiated or intensified, leading to the reduction of their lifetime (Fabiani 2013, Notingher 2005).

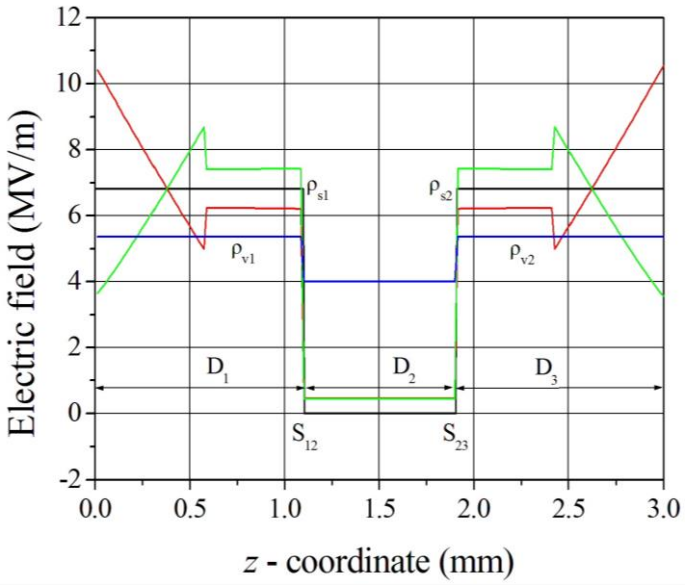


Fig. 18. Variation of electric field with z – coordinate for unaged samples: $\rho_v = \rho_s = 0$ (blue curve), ρ_{s1} = 0.12 mC/m^2 and ρ_{s2} = - 0.12 mC/m^2 and $\rho_{v01} = \rho v_{02} = 0$ (black curve), ρ_{s1} = 0.12 mC/m^2 and ρ_{s2} = - 0.12 mC/m^2 and ρ_{v01} = 2 C/m^3 and ρ_{v02} = - 2 C/m^3 (red curve) and ρ_{s1} = 0.12 mC/m^2 and ρ_{s2} = - 0.12 mC/m^2 and ρ_{v01} = - 2 C/m^3 and ρ_{v02} = 2 C/m^3 (green curve)

(U = 15 kV, $\rho_{v1} = \rho_{v01}e^{-C_1 z}$, $\rho_{v2} = \rho_{v02}e^{-C_2(z_{max}-z)}$).

Thermal aging of the samples caused an important modification of the electrical conductivity and a lesser one of their permittivity. Therefore, the time constants that characterize the charge accumulation process at the interfaces (τ_1 and τ_2) were modified, but the electric field variations in the absence and presence of the space charge are similar to those in unaged samples.

The values of the volume charge density were chosen according to those presented in other papers (Boyer 2013, Morsius 2013, Stancu 2013a) and the superficial charge ones were computed. It should be noted that for electric field computation (and, thus, ρ_{s1} and ρ_{s2}) the increase of the conductivity with the electric field (Stancu 2016) and temperature (Jeroense 1998) it was not considered. Verification of these values will be done, in the future, by measuring the space charge values (by Thermal Step Method), both on flat and cylindrical samples and by taking into consideration the variation of the conductivity with the electric field strength.

6. CONCLUSIONS

A theoretical and experimental study regarding the generation of the space charge in DC cable joints and its effect on the electric field and electrical degradation process is presented. It is shown that the volume space charge occurs due to the technological processes, ageing and injection from electrodes when the voltage is applied.

The flat multilayer insulations present space charge that is assigned, both in the volume and at the interfaces of the homogeneous areas.

The proposed analytical model of the electric field and charge density allows calculating their values in the absence of the volume space charge. These values are used for the numerical computation of the electric field in the presence of charge, both in volume and at the interfaces of the joint model.

Space charge accumulation in multilayer insulations of the DC joints leads to the intensification of the electric field and to occurrence of higher fields than those of the partial discharges and electrical trees inception values.

Results presented in this paper are obtained on flat multilayer samples. The results obtained on cylindrical samples and the dependency of the conductivity with the electric field strength will be presented in a future paper.

ACKNOWLEDGMENTS

The work has been funded by the Ministry of Education through the PN-II-RU-TE-2014-4-0280 Project and Sectorial Operational Programme Human Resources Development 2007-2013 of the Ministry of European Funds through the Financial Agreement POSDRU/159/1.5/S/132395.

REFERENCES

Abou-Dakka, M, Bamji, S & Bulinski, A 1997, "Space Charge Distribution Measurements in XLPE and EPR", *Proceedings of IEEE Conf. Electr. Insul. Dielectr. Phenomena (CEIDP)*, Mineapolis, Minnesota, USA, pp. 23-27.

Abou-Dakka, M, Bulinski, A & S. Bamji, S 2004, "Space Charge Development and Breakdown in XLPE under DC field", *IEEE Trans. Dielectr. Electr. Insul*., Vol. 11, pp. 41-49.

Aghazadeh, A 2014, "Convertion HVAC into HVDC of Power Transmission Lines with Using Voltage Source Converter", *Proceedings of 29th Power System Conference* (*PSC* 2014), Tehran, Iran, pp.1-7.

Agnel, S, Castellon, J & Notingher, P jr. 2013, "Space Charge Measurements in Cable Insulating Materials: from Research Laboratory to Industrial Application", *Proceedings of 8th International Conference on Insulated Power Cables - Jicable'*13, Paris, 19-23 June, Paper 2.2.

Amyot, M & Fournier, D 2001, „Influence of Thermal Cycling on the Cable- Joint Interfacial Pressure", *Proceedings of IEEE 7th International Conference on Solid Dielectrics*, pp. 35-38.

Bartnikas, R & Srivastava, KD 2000, *Power and Communication Cables*, IEEE PRESS, New York.

Bodega, R, Morshuis, P, Nilsson, U & Smit, GJ 2006 a, „Polarization Mechanisms of Flat XLPE-EPR Interfaces", *Proceedings of Nordic Insulation Symposium*, pp. 224-227.

Bodega, R 2006 b, *Space Charge Accumulation in Polymeric High Voltage DC Cable Systems*, Ph.D Thesis, Delft University, The Netherlands.

Boggs, S 2004, "A Rational Consideration of Space Charge", *IEEE Electr. Insul. Magazine*, Vol. 20, pp. 22-27.

Boyer, L 2013, "Cable Research Testing", *Proceedings of 8th International Conference on Insulated Power Cables - Jicable'*13, Paris, 19-23 June, Paper 5.1.

Castellon, J, Notingher, P jr., Agnel, S, Toureille, A, Matallana, J, Janah, H, Mirebeau, P & Sy, D 2005, "Industrial Installation for Voltage-on Space Charge Measurements in HVDC Cables", *Conference Record of the 2005 IEEE IAS Annual Meeting*, Vol. 2, pp. 1112-1118.

Europacable, 2011, "An Introduction to High Voltage Direct Current (HVDC) Underground Cables", pp. 1-13.

Fabiani, D, Montanari GC 2013, "HVDC Aging Modeling for Polymeric Cable: An Overview", *Proceedings of 8th International Conference on Insulated Power Cables - Jicable'*13, Paris, 19-23 June, Paper 3.3.

Fu, M, Chen, G, Dissado, LA & Fothergill, JC 2007, "Influence of Thermal Treatment and Residues on Space Charge Accumulation in XLPE for DC Power Cable Application", *IEEE Trans. Dielectr. Electr. Insul.*, Vol. 14, No. 1, pp. 53-64.

Hjertberg, T, Englund, V, Hagstrand, P-O, Loyens, W, Nilsson, U, Smedberg, A 2013, "Materials for HVDC Cables", *Proceedings of 8th International Conference on Insulated Power Cables - Jicable'*13, Paris, 19-23 June, Paper 2.1.

Hondaa, P 2013, "Qualification Testing of Synthetic Cable Systems", *Proceedings of 8th International Conference on Insulated Power Cables - Jicable'*13, Paris, 19-23 June, Paper 5.2.

Jeroense, M & Morshuis, P 1998, "Electric Fields in HVDC Paper-Insulated Cables", *IEEE Transactions on Dielectr. Electr. Insul.*, Vol. 5, No. 2, p. 225 -236.

Jeroense, M, Saltzer, M & Ghorbani, H 2013, "Technical Challenges Linked to HVDC Cable Development", *Proceedings of 8th International Conference on Insulated Power Cables - Jicable'*13, Paris, 19-23 June, Paper 1.1.

Kim, C, Sood,V, Jang, G, Lim, S & Lee,S 2009, „*HVDC Transmission: Power Conversion Applications in Power Systems*", Wiley IEEE Press.

Kreutzer, U 2015, "Researching a Revolution", https://www.siemens.com/innovation/en/home/pictures-of-the-future/research-and-management/innovations-energy-systems-of-the-future.html

Larruskain, DM, Zamora, I, Mazon, AJ, Abarrategui, O & Monasterio J 2005, "Transmission and Distribution Networks: AC versus DC", *Proceedings of 9th Congr. Hisp-Luso de Ing. Electr.* (9*CHLIE*), Marbella (Spain).

Montanari, GC & Morshuis, PHF, 2005, "Space Charge Phenomenology on Polymeric Insulating Materials", *IEEE Trans. Dielectr. Electr. Insul*., Vol. 12, No. 4, pp. 754-767.

Morshuis, P, Kochetov, R & Tsekmes, I 2013, "Interfaces at DC – Electrical and Thermal Barriers", *Proceedings of 8th International Conference on Insulated Power Cables - Jicable'*13, Paris, 19-23 June, Paper 2.3.

Namouchi, F, Smaoui, H, Guermazi, H & Zerrouki, C 2007, „Study of Thermal Aging Effect on Space Charge in Poly(methyl methacrylate)", *European Polymer Journal*, No. 43, pp. 4821-4829.

Notingher, P jr. 2000, "*Etude des charges d`espace et des pertes dans l`isolant des câbles de transport d`énergie électrique en vue de l`accroissement du rendement*", Ph.D Thesis, Université Montpellier 2, France.

Notingher, P jr., Agnel, S & Toureille, A 2001, "The Thermal Step Method for Space Charge Measurements under Applied DC Field", *IEEE Trans. on Dielectrics and Electrical Insulation*, Vol. 8, No. 6, pp. 985-994.

Notingher, P jr., Toureille, A, Agnel, S, Castellon, J 2009 „Determination of Electric Field and Space Charge in the Insulation of Power Cables with the Thermal Step Method and a New Mathematical Processing'', *IEEE Transactions on Industry Applications*, Vol. 45, No.1, pp. 67 – 74

Notingher, PV 2005, *Materials for electrotechnics*, POLITEHNICA PRESS, Bucharest.

Notingher, PV, Dumitran, LM & Busoi, SA 2010, „Lifetime Estimation of Composite Insulations by Absorption/Resorption Currents Method", *Revue Roum. Sci. Tech. - Electr. Et Energ*., Vol. 55, No. 4, pp. 365–374.

Parpal, J-L, Awad, R, Choquette, M, Becker, J, Hiivala, L, Chatterjee, S, Kojima, T, Rosevear, RD & Morelli, O 1996, "Prequalification Tests of 345 kV XLPE Cable System at IREQ", *Proceedings of*

Conference Record of the IEEE International Symposium om Electrical Insulation, Montreal, Quebec, Canada, pp. 616-615.

Pfisterer Cable Systems 2015**,** *Cable fittings for high voltage networks, Online Catalogue*, http://products.pfisterer.com/procat_international/catalog/

Seghier, T, Mahi, D & Lebey, T 2010, „The effect of space charge on partial discharges inception voltage in air gaps within high density polyethylene", *Courrier du Savoir*, No. 10, pp. 35-41.

Sharif, S & Kasicki, A 2012, „The Environmental Impacts of UHVDC Power Transmission Proposed Line from Iraq to Europe through Turkey", *Journal of Purity, Utility Reaction and Environment*, Vol.1, No.9, pp. 460-471.

Stancu, C 2008, "*Caractérisation de l'état de vieillissement des isolations polymères par la mesure d'arborescences et de charges d'espace*", Ph.D Thesis, Politehnica University of Bucharest (Romania) and Université Montpellier 2 (France).

Stancu, C, Notingher, PV, Notingher P jr. & Plopeanu M 2009, "Water Tree Influence on Space Charge Distribution and on the Residual Electric Field in Polyethylene Insulation", *Journal of Electrical and Electronics Engineering*, Vol.2, No.2, pp. 89-94.

Stancu, C, Notingher, VP, & Plopeanu, MG 2011, „Influence of Water Trees on Breakdown Voltage of Polymeric Cables Insulations", *Journal of International Scientific Publications: Materials, Methods & Technologies* ,Vol. 5. Part 2, pp. 101-116.

Stancu, C, Notingher, PV & Notingher, Pjr 2013 a, „Computation of the Electric Field in Aged Underground Medium Voltage Cable Insulation", *IEEE Transactions on Dielectrics and Electrical Insulation*, Vol. 20, No. 5, pp. 1530-1539.

Stancu, C & Notingher, PV 2013 b, „Electrical Stresses of DC Cable Insulation, *Journal of International Scientific Publications: Materials, Methods & Technologies*, Vol. 7, Part 1, pp. 106 - 123.

Stancu, C, Notingher, PV, Constantin, A, Cernat, A, Notingher PJr & Lungulescu, M 2014, " Space Charge in Thermally Aged Multilayer Joints", *Proceedings of 9eme Congres de la Societe Francaise d'Electrostatique,* pp. 360-365.

Stancu, C, Notingher, PV, Notingher, Pjr & Lungulescu M 2016, „Space Charge and Electric Field in Thermally Aged Multilayer Joints Model", *IEEE Transactions on Dielectrics and Electrical Insulation* (To be published).

Suh, KS, Hwang, SJ, Noh, JS & Tanaka, T 1994, "Effects of Constituents of XLPE in the Formation of Space Charge", *IEEE Trans. Dielectr. Electr. Insul*., Vol. 1, pp. 1077-1083.

Taranu, LV, Notingher, PV & Stancu C 2015, Influence of the Electric Charge Accumulated at the Inhomogeneous Insulation Interfaces of Electrical Equipment on the Electric Field Distribution, *Proceedings of Electrical Machines National Symposium* (*EMS*'15), Bucharest, Romania, Paper 3, pp. 1-14.

Toureille, A, Reboul, JP & Merle, P 1991, "Détermination des densités de charge d'espace dans les isolants solides par la méthode de l'onde thermique", *J. Physique III*, Vol. 1, pp. 111-123.

Tsekmes, I 2012 „*Electrical characterization of polymeric dc mini-cables by means of space charge & conduction current measurements*", PhD Thesis, Delft University of Technology.

UEFISCDI, 2016, "*Reduction of Space Charge in Composite Insulations of High Voltage DC Joints*", Code: PN-II-RU-TE-2014-4-0280, http://amotion.pub.ro/stancu/en/index.html.

Ve, TA, F. Mauseth, F & Ildstad, E 2013, „Space Charge Accumulation in XLPE versus Temperature and Water Content", *Proceedings of Nordic Insulation Symposium*, Trondheim, Norvege, pp. 15-18.